A Kinetic Model of Proton Transport in a Multi-Redox Center Protein: Cytochrome *c* Oxidase

Johannes Srajer[1,2], Andreas Schwaighofer[1], David M. Hildenbrandt[1], Asmorom Kibrom[1] and Renate L.C. Naumann[*1]

[1]Austrian Institute of Technology GmbH, AIT, Donau-City Str. 1, 1220 Vienna

[2]CEST Center of Electrochemical Surface Technology, Viktor-Kaplan-Strasse 2, 2700 Wiener Neustadt, Austria

*e-mail: renate.naumann@ait.ac.at

The final version of this accepted manuscript was published in Progress in Reaction Kinetics and Mechanism. DOI: 10.3184/146867812X13558465325118.

Abstract

We use chemical reaction kinetics to explore the stepwise electron and proton transfer reactions of cytochrome *c* oxidase (C*c*O) from *R. sphaeroides*. Proton transport coupled to electron transport is investigated in terms of a sequence of protonation-dependent second order redox reactions. Thereby, we assume fixed rather than shifting dissociation constants of the redox sites. Proton transport can thus be simulated particularly when separate proton uptake and release sites are assumed rather than the same proton pump site for every ET step. In order to test these assumptions, we make use of a model system introduced earlier, which allows to study direct ET of redox enzymes by electrochemistry. A four-electron transfer model of C*c*O had been developed according to which electrons are transferred from the electrode to Cu_A. Thereafter, electrons are transferred along the sequence heme *a*, heme a_3 and Cu_B. In the present investigation we consider protonation equilibria of the oxidized and reduced species for each of the four centers. Moreover, we add oxygen/H_2O as the terminal (fifth) redox couple including protonation of reduced oxygen to water. Finally we arrive at a kinetic model comprising five protonation-dependent redox couples. The results from the simulations are directly compared with experimental data obtained in the absence and presence of oxygen. As a result, we can show that proton pumping can be modeled in terms of protonation-dependent redox kinetics.

Keywords: proton pump, protonation-dependent chemical reaction kinetics, second order redox reaction, metalloprotein, master equation

1. Introduction

Cytochrome *c* Oxidase (C*c*O) is the final complex of the respiratory chain. Its purpose is to use the energy gained by the reduction of oxygen to water to pump protons against a difference of electrochemical potentials across the mitochondrial inner membrane. This pumping is achieved by coupling a number of electron (ET) and proton transfer (PT) steps. The stepwise transfer is under debate since CcO has been recognized as a proton pump more than three decades ago.[1-2,3] According to current view, the gradual increase of the pK value during each ET step leads to the transfer of a proton to the proton loading site (PLS), which is separated from the site where oxygen chemistry occurs.[4-7] After the transfer of a proton to the PLS, another proton is taken up for the chemical reaction in the catalytic site. Electrostatic repulsion from this second proton will then expel the proton out of the PLS. This view is hard to challenge experimentally, particularly since few methods are available to follow ET and HT steps during an entire catalytic cycle, see however reference 8. A convenient way to study proton-coupled ET is chemical reaction kinetics initiated by electrochemistry.[9-12] In this study, we make use of a model system developed earlier, which permits direct ET to redox enzymes.[13] This system comprises C*c*O from *R. sphaeroides* tethered to an electrode via a his-tag attached to subunit (SU) II followed by reconstitution into a protein-tethered bilayer lipid membrane (ptBLM). The benefit of this system is the accessibility of the internal redox centers avoiding the diffusion limitation of mediators. A further advantage inherent in the geometry of the ptBLM is the hydrophilic layer between the electrode and the lipid membrane provided by the tether molecules. The experimental benefit is the sensitivity of the small interstitial reservoir (~0.2 nL cm^{-2}) to changes in proton concentration as a result of enzyme activity. Thus, this methodology presents a new approach to separately examine proton and electron transfer reactions in membrane proteins, see the schematics of the model system (Fig. 1).

Previous studies have made it highly likely that electrons are transferred from the electrode directly to Cu_A. A sequential four-electron transfer model had been designed according to which electrons are then transferred along the sequence Cu_A, heme *a*, heme a_3 and Cu_B.[14] In the presence of oxygen, the enzyme displays enzymatic activity indicated by amplified electron as well as proton currents.[15]

In the present investigation, we extend this four-electron transfer model in two steps. In the first step we consider protonation equilibria of the oxidized and reduced species for each of the four centers. In the second step we add oxygen/H_2O as the terminal (fifth) redox couple including protonation of reduced oxygen to water. Finally, we arrive at a kinetic model comprising five redox couples describing a string of second order reactions with protonations. The model will be tested using cyclic voltammetry data of the C*c*O in the absence and presence of oxygen.

2. Kinetic Model

The sequential four electron transfer model of C*c*O, comprising the redox sites $\mathrm{Cu_A}$, heme a, heme a_3 and $\mathrm{Cu_B}$, has been developed before.[14] Each site is either in the reduced (r) or in the oxidized (o) state. The model therefore results in $2^4 = 16$ possible redox states of the enzyme. In order to simulate internal processes within the enzyme, time-dependent density functional theory is used, which is based on the local equilibrium assumption.[16] Recent developments show that this can also be applied to far from equilibrium dynamics under time-dependent driving signals such as cyclic voltammetry.[17] Instead of using an electrostatic approach calculating the Coulomb forces for a fixed spatial dilatation of the enzyme, we employ chemical reaction kinetics based on a modified Nernst equation, taking into account protonation equilibria. In our formulation we describe the behavior of the enzyme by rate constants, standard redox potentials and acid dissociation constants.

2.1 General Concepts

Since we are interested in dynamic processes within a single complex, it is sufficient to define a probability P_i for every single redox state i ($i = 1,\ldots,16$) of the enzyme. The temporal evolution of this system is governed by the master equation

$$\frac{d}{dt}P_i = \sum_{j\neq i} k_{ij}P_i - k_{ji}P_j, \qquad (1)$$

where k_{ij} and k_{ji} are the forward and backward reaction rates for the transition from redox state i into state j. The relation between these reaction rates is defined by the equilibrium constant $K = \frac{k_{ij}}{k_{ji}}$. Since we are dealing with a single complex, the condition

$$\sum_{i=1}^{16} P_i = 1 \qquad (2)$$

holds at any time.

2.1.1 Redox Reactions and Protonation

Considering a single redox couple, protonation / deprotonation in the course of the transition from the oxidized to the reduced state can take place in four different ways, dependent on the dissociation constants K_m^o and K_m^r of the oxidized and reduced state, respectively (Fig. 2).
Since spectroscopic methods distinguishing between protonated and deprotonated species are often not available, we adopted a concept developed by D. Walz for all kinds of redox processes associated with ligands.[18] This concept comprises total reduced and oxidized species as the sum of ligated and unligated species. Translated into the realm of protonations this means considering total species as the sum of protonated and deprotonated species, resulting in Eqs. (3) and (4) for the reduced and oxidized form, respectively

$$[r_m^t] = [r_m] + [Hr_m] = [r_m](1 + 10^{pK_m^r - pH}) \text{ and} \qquad (3)$$

$$[o_m^t] = [o_m] + [Ho_m] = [o_m](1 + 10^{pK_m^o - pH}), \qquad (4)$$

Insertion of Eqs. (3) and (4) into the Nernst equation yields

$$E = E_m^0 + \frac{RT}{nF}\ln\frac{[o_m^t]}{[r_m^t]} + \frac{RT}{nF}\ln\frac{1+10^{pK_m^r - pH}}{1+10^{pK_m^o - pH}}, \qquad (5)$$

with E as the electrode potential E^0 as the standard redox potential both defined in aqueous solution versus standard hydrogen electrode (SHE) as the reference point, T as the temperature, n as the number of electrons involved in this process and R and F are the universal gas and Faraday constant. According to Eq. (5), the electrode potential E depends not only on the ratio between the redox states, but also on pH and the pK values of the oxidized and reduced species. In biochemical

literature, the first and third term are often combined to yield the midpoint potential E^m, defined by Eq (6).[12,18]

$$E_m^m = E_m^0 + \frac{RT}{nF}\ln\frac{1+10^{pK_m^r-pH}}{1+10^{pK_m^o-pH}}, \quad (6)$$

Due to the second term in Eq. (6), the midpoint potential is pH dependent.

We now proceed to consider the interaction between two such protonation-dependent redox couples, each one defined by the modified Nernst Eq. (5) (see Fig. 3).

We begin with the second order reaction equation written likewise in terms of total species

$$[r_l^t] + [o_m^t] \rightleftharpoons [o_l^t] + [r_m^t], \qquad (7)$$

yielding the equilibrium constant of this reaction

$$K = \frac{k_{lm}}{k_{ml}} = \frac{[o_l^t][r_m^t]}{[r_l^t][o_m^t]}, \qquad (8)$$

which determines the ratio between forward and backward reaction rates. Insertion of Eq. (5), that is valid for each of the single redox centers *l* and *m*, the equilibrium constant for this reaction follows to

$$K = \frac{k_{lm}}{k_{ml}} = e^{\frac{nF(E_m^0-E_l^0)}{RT}}\,\frac{(1+10^{pK_l^o-pH})}{(1+10^{pK_l^r-pH})}\frac{(1+10^{pK_m^r-pH})}{(1+10^{pK_m^o-pH})}. \qquad (9)$$

From Eqs. (8) and (9) the flow of electrons J_{kl} between centers *l* and *m* can be calculated, once the forward reaction rate has been identified, e.g. by independent measurements,

$$J_{lm} = \Gamma\ A\left(k_{lm}P_i - k_{lm}\ e^{\frac{nF(E_l^0-E_m^0)}{RT}}\ \frac{(1+10^{pK_l^r-pH})}{(1+10^{pK_l^o-pH})}\frac{(1+10^{pK_m^o-pH})}{(1+10^{pK_m^r-pH})}P_j\right), \qquad (10)$$

using Γ, the surface concentration of the enzyme and A the surface area. Note that introducing Eq. (10), we are able to take into account the pK values of all of the species possibly involved in a second order reaction given by Eq. (7).

2.1.2 Transition rates of protons

The number of protons taken up or released in a second order reaction depends on the difference in magnitude of the dissociation constants of reduced and oxidized species. Assuming the equilibrium condition for all kinds of protonations/deprotonations, we derive probabilities of protons being taken up or released in a particular redox reaction. The transition rates of protons are then obtained by multiplying the flow of electrons calculated in Eq. (10) with these probabilities. For example, we can deduce from the dissociation constants that the probabilities of the reduced species to be in the deprotonated and protonated state are $\frac{1}{1+10^{pK^r-pH}}$ and $\frac{1}{1+10^{pH-pK^r}}$, respectively. Hence, the probability of a proton being associated in the course of reduction P_m^{up} of a single redox couple m follows to

$$P_m^{up} = \frac{1}{1+10^{pK_m^o-pH}} \; \frac{1}{1+10^{pH-pK_m^r}}. \tag{11}$$

In the case of a second order reaction, the probabilities of species being protonated or deprotonated have to be taken into account for both redox couples. This leads to a number of 16 different combinations depicted in Fig. 3. For example, transition 1 combined with 6 and transition 2 with 8 yields an uptake of a proton. Transition 1 combined with 7 and transition 3 with 5 yields a release and transition 3 combined with 6 and transition 4 with 8 yields a concomitant ET and HT. The total number of protons in every transition is then obtained by the sum of the transition probabilities having the same result. For further details, see the supplementary information.

2.1.3 Electrode reactions

The treatment so far is only applicable to second order chemical reactions. In our model system, however, $\mathrm{Cu_A}$, the first redox center is connected to the electrode. Hence, in this case, the rate of electron transfer to $\mathrm{Cu_A}$ depends on the applied potential E according to the Butler-Volmer equation.[19] Inserting midpoint potentials (Eq. (6)), in order to take into account protonation constants of reduced and oxidized species, the current i^e resulting from the electron transfer to $\mathrm{Cu_A}$ follows to

$$i^e = -FAk_e\Gamma\sum_{i\neq j}\left(P_i e^{\frac{F\alpha(E_1^0-E)}{RT}}\left(\frac{1+10^{pK_1^T-pH}}{1+10^{pK_1^O-pH}}\right)^{\alpha} - P_j e^{\frac{-F(1-\alpha)(E_1^0-E)}{RT}}\left(\frac{1+10^{pK_1^T-pH}}{1+10^{pK_1^O-pH}}\right)^{-(1-\alpha)}\right), \quad (12)$$

with the surface area A of the electrode, the standard rate constant k_e of the electron transfer, the surface concentration of the enzyme Γ and the charge transfer coefficient α. The reduction of $\mathrm{Cu_A}$ is a one electron transfer process so that $n = 1$ is already inserted in Eq. (12). The same formalism is also used for protons, which are reduced to hydrogen at the electrode. These protons are the so-called pumped protons, which arrive at the electrode in the course of enzyme turnover. Two electrons are used to reduce two protons to a hydrogen molecule $\mathrm{H_2}$. The current i^H flowing in this process is calculated according to

$$i^H = -F\ A\ k_{e,H}\left([H]\ e^{\frac{F\alpha(E^0-E)}{R\ T}}\right), \quad (13)$$

with the concentration of protons $[H]$ in the aqueous phase, the rate constant $k_{e,H}$ and the standard potential E^0 of molecular hydrogen formation, which is shifted by -0.39 Volts versus SHE, due to kinetic limitations at the gold electrode.[20] The dependence on the partial pressure of $\mathrm{H_2}$ is negligible due to the rapid diffusion of $\mathrm{H_2}$ into the surrounding air. Both electrode reactions contribute to the current measured in experiments $i^{exp} = i^e + i^H$. The ratio between the two kinds of currents yields the number of protons pumped per electron.

2.2 Electrochemical Model System

The complete model system is depicted schematically in Fig. 4. Under anaerobic conditions only the pathway indicated by electrochemical reduction are active indicated by the black arrows, whereas under aerobic conditions the model is expanded to take into account also enzymatic reoxidation indicated by the green arrows. Taken under anaerobic conditions, the model comprises the electrochemical electron uptake by $\mathrm{Cu_A}$ coupled to a series of second order electron exchange reactions to heme a, heme a_3 and $\mathrm{Cu_B}$. This sequential four ET model had already been discussed previously. The four redox centers can be present in the reduced and oxidized state, indicated by

the letters r and o, respectively. Electrons are taken up by the enzyme electrochemically, but only via the first electron acceptor, $\mathrm{Cu_A}$.[14]

Considering protonations, in principle all of the reduced and oxidized species can be protonated depending on their individual pK^r and pK^o values. This increases the number of possible redox and protonation states to 256 different states, which cannot be reflected in the schematic shown in Figure 4. In the presence of oxygen, the enzymatic turnover has to be taken into account. To this end, oxygen is considered as a fifth redox couple, exchanging electrons and protons in a further second order reaction with reduced $\mathrm{Cu_B}$. One-electron transfer steps are considered, thus dividing the reduction of one $\mathrm{O_2}$ molecule into four steps consuming $\frac{1}{2}\mathrm{O} + 1\ \mathrm{H}$ yielding $\frac{1}{2}\mathrm{H_2O}$ each. Four such steps yield one full cycle of the C*c*O, using four protons (H) and one oxygen molecule ($\mathrm{O_2}$) to form two water molecules ($2\ \mathrm{H_2O}$). Even though this is still a simplified model, it enables us to simulate the sequential reduction of the redox centers coupled to reoxidation by oxygen, thus mimicking a full enzymatic cycle.

3. Materials and Methods

3.1 Immobilization of the protein

Immobilization of C*c*O on the template stripped gold (TSG)[21] electrodes was performed as described in detail by Nowak et al..[22] Briefly, C*c*O from *Rhodobacter sphaeroides* with a his-tag engineered to the C-terminus of subunit II was expressed and purified according to Hiser and Ferguson-Miller.[23] TSG electrodes were provided with a self assembled monolayer of a mixture of dithiobis (nitriloacetic acid butylamidyl propionate (DTNTA) and dithiobis (propionic acid) (DTP) in a mole ratio of 0.2. After loading the NTA-functionalized surface with Ni^{2+}, C*c*O dissolved in dodecyl β-D-maltoside (DDM)-phosphate-buffer (0.05 M K_2HPO_4, 0.1 M KCl, pH=8, 0.1% DDM) was adsorbed at a final concentration of 100 nM. Dialysis was performed in-situ in a DiPhyPC solution (40 µM) in DDM-phosphate buffer by adding biobeads (Bio-Rad Laboratories GmbH, Munich, Germany) to the lipid-detergent solution.

3.2 Electrochemical Methods

Electrochemical measurements were performed using an Autolab instrument (PGSTAT302 with GPES 4.9) with an ECD-module amplifier for low-currents, an ADC750 module for rapid scan measurements and a SCAN-GEN module for analog potential scanning. Cyclic voltammetry experiments were conducted with IR drop compensation. Measurements were performed in a buffer solution containing 0.05 M K_2HPO_4, 0.1 M KCl, pH=8. Under anaerobic conditions, the buffer solution was flushed with Ar and an oxygen trap consisting of glucose (0.3 %w/w), glucose oxidase (75 µg/ml) and catalase (12.5 µg/ml) was added. Under aerobic conditions the buffer solution was flushed with oxygen. Thereafter, up to 30 CVs were taken until the CV had reached steady state regarding peak position and current density. All electrochemical measurements were taken in a three electrode configuration with TSG as the working electrode, a $Ag|AgCl,KCl_{sat}$ reference, and a platinum wire as the counter electrode. All electrode potentials are quoted versus SHE.

3.3 Computational Methods

The system of 16 differential equations, described by the master equation are solved numerically using the solver ode15s of the commercially available software package MATLAB R2011a®.

4. Results and Discussion

In order to explore the impact of protonations on our four-electron transfer model (see Fig. 4) we used the same data sets presented in the context of our previous studies.[14,22] CVs taken under strictly anaerobic conditions had shown peaks in the range of 200 to 600 mV, corresponding to midpoint potentials of redox centers known from equilibrium titrations (see Fig. 5A).[24] In an air-saturated solution, the enzyme had been shown to work under turnover conditions, indicated by two peaks appearing at around -200 mV and −500 mV exhibiting an increased

current density (Fig. 5B). These peaks had been attributed to repeated electron and proton transfer. [1313] Surprisingly, the electron transfer peak was shifted by more than 400 mV in the negative direction vs. known midpoint potentials. Returning to anaerobic conditions, we had found that the peak at around -200 mV persisted for a certain period of time (Fig. 5C), before the enzyme relaxes back to the original anaerobic state (Fig. 5A). We had deduced from these results that the enzyme undergoes a transition from a non-activated to an activated conformational state, equivalent to the transition from the resting to the pulsed state when the C*c*O reconstituted in liposomes is subjected to oxygen pulses.[22] The negative shift of the electron transfer peak had been confirmed by equilibrium potentiometric titrations of the activated enzyme followed by FTIR spectroscopy.[15,22]

Electron and proton currents were calculated using Eqs. (13) and (14). CVs were simulated based on triangularly shaped changes of applied voltages as a function of time. Since a large number of parameters have to be considered, some of them were fixed to values adopted from previous studies such as electrochemical rate constants, surface concentrations of C*c*O, and forward reaction rates. Redox potentials were adopted from equilibrium potentiometric titrations followed by UV/VIS and FTIR measurements.[24] The list of all fixed parameters can be found in the supplementary information. Since the focus of this study is protonation, we varied the dissociation constants of reduced and oxidized species according to Table 1.

Table 1: Variation of acid dissociation constants. Every redox center has two acid dissociation constants for the reduced and the oxidized species, respectively.

variation	Cu_A		heme a		heme a_3		Cu_B	
no.	pK_1^r	pK_1^o	pK_2^r	pK_2^o	pK_3^r	pK_3^o	pK_4^r	pK_4^o
V1	0	0	10	0	10	0	3	0
V2	0	0	3	0	10	0	3	0
V3	0	0	3	0	10	0	9	0

In a first attempt to simulate the CVs of the non-activated anaerobic C*c*O (Fig. 5A), pK^r values were estimated according to the mechanisms of proton uptake and release described in section 2.1.2. pK^o values are very hard to estimate and therefore they were set to zero. Using parameter set V1 proton uptake and release is assumed in reactions between Cu_A and heme *a*, and between heme a_3 and Cu_B, respectively, whereas concomitant electron and proton transfer is assumed between heme *a* and heme a_3. E^m of Cu_A is assumed not to be pH dependent. The first positive peak in Fig. 5A corresponds to the redox potential of Cu_A of about 250 mV. The second positive peak located at 520 mV cannot be attributed to any of the known midpoint potentials of C*c*O.[24] Using the modified model taking into account parameter set V1 results in an additional peak shifted in the positive direction to 470 mV (Fig. 6A) in good agreement with the measurement (Fig. 5B). Previous modeling studies that do not consider protonations have not been able to describe this phenomenon.[14] Extending the model to include oxygen reduction (Fig. 4) and keeping the parameter set V1 yields the simulated CV shown in Fig. 6B. An overall catalytic current density 60 µA cm^{-2} is recognized as well as a current due to proton reduction at the electrode of about 30 µA cm^{-2}, which is in agreement with measured values. The proton current indicates proton pumping, which is the result of proton uptake and release in the reaction kinetics. The overshooting proton peak at a potential of about 65 mV (Fig. 6B) is an artifact due to rapid changes of the pH in the interstitial volume of only 0.24 nl cm^{-2}, between the electrode and the lipid membrane.[13] Hence, we consider constant currents only, although peak shaped currents are seen in the experiments. They are due to diffusion based depletion of oxygen and protons, which have not been taken into account in the simulation (see Fig. 6B).

Changing the parameter set to V2, thereby decreasing pK^r_3 of heme *a* to $pK^r_3 = 3$, we assume a further proton release step on the level of ET between heme *a* and a_3. As a result we still see electron and proton currents equal in magnitude under aerobic conditions, however, too high as compared to the measured data (Fig. 6D). Also the simulated CV under anaerobic conditions do no longer compare favorably with the measured data. The peak due to reduction of Cu_A (262 mV) is

still close to 250 mV, however, a prominent peak appears at 355 mV and a smaller one at 475 mV (Fig. 6C). Further changing the parameter set to V3, thereby deliberately assuming pK^r_4 of Cu_B being $pK^r_4 = 9$, attributed to the PLS in previous studies.[5-6,25] This parameter set results in no proton current at all, and an ET current of around 60 µA cm^{-2} density (Fig. 6F). The anaerobic case shows again a peak at 259 mV due to Cu_A, however, two more positive peaks at 343 and 442 mV, different from the measured CV, exhibiting a single more positive peak at 520 mV (Fig. 5B).

The best result so far has been obtained with parameter set V1, at least as far as proton and electron currents is concerned. This parameter set comprises ET occurring concomitantly with HT between heme *a* and heme a_3, an overall charge balanced process. This would explain not only the fast ET rate measured between these redox centers but also that this ET does not seem to contribute to the generation of membrane potential of the C*c*O.[8]

The negative shift of the ET and HT peaks under aerobic conditions, however, can only be simulated by assuming equilibrium potentials of the activated enzyme shifted to negative potentials, in agreement wuth our previous modeling and FTIR studies, see also the supplementary Information.[14,22] Using pK^r values according to the parameter setting V1 results in a simulated CV with ET and HP currents equal in magnitude and, both shifted to around -200 mV (Fig. 6H), in reasonable agreement with the measurement (Fig. 5B). Peaks in the simulated CV under anaerobic conditions are equally shifted in the negative direction, which is consistent with respective measured CVs of the activated rather than the non-activated enzyme (Fig. 6G).

For a more accurate determination of *pK* values including pK^o, we are currently working on an adequate parameter optimization routine, in order to deal with the number of free parameters.

5. Conclusions

The simulations show that the concept of a string of second order reactions including protonations appears to reflect the behavior of the C*c*O, at least in principle, regarding catalytic currents as well as proton translocation. Notably, this concept is based on constant *pK* values and standard redox

potentials rather than *pK* or E^0 changing in the course of a redox reaction as assumed in previous studies.[4,6-7,26] E^m may change as a function of pH, though. As far as *pK* and E^0 values are concerned, however, there is no reason to believe that the principles described by Eqs. (9) and (10) work differently in a protein as compared to an ordinary chemical reaction, see e.g. refs [9,12,27-28]. Proton pumping can thus be simulated particularly when separate proton uptake and release sites are assumed rather than the same proton pump site for every ET step. In this regard, there are similarities with another kinetic model also comprising four ET and four PT sites.[25] Different from this model, however, in order for pumping to take place in our model, the pK of the release site is required to be smaller than that of the uptake site (see parameter set V3 compared to V1). The low pK values could be due to a yet unidentified anionic group coupled to Cu_B reduction. A further requirement for an effective proton pumping is considering oxygen/H_2O as a fifth redox couple including the ionic product of water. This gives rise to a final ET and HT uptake rather than a separate chemical reaction. We have to bear in mind, however, that we are still using a simplified model, particularly regarding the reactions with oxygen. The net result, however, should be the same, at least as far as proton pumping is concerned.

Acknowledgment

We gratefully acknowledge the invaluable advice and assistance over the years of Prof. Dieter Walz, Biozentrum, University of Basel, Switzerland. Likewise, we are very grateful to Prof. Shelagh Ferguson-Miller and Carrie Hiser, Michigan State University, East Lansing MI 48824, USA, for inspiring discussions and for providing us with high-quality preparations of C*c*O from *R. sphaeroides*.

References

(1) Wikstrom, M.; Verkhovsky, M. I. *Biochim. Biophys. Acta, Bioenerg.* **2007**, *1767*, 1200-1214.

(2) Brzezinski, P.; Gennis, R. *J. Bioenerg. Biomembr.* **2008**, *40*, 521-531.

(3) Wikstrom, M. K. F. *Nature* **1977**, *266*, 271-273.

(4) Popovic, D. M.; Stuchebrukhov, A. A. *FEBS Lett.* **2004**, *566*, 126-130.

(5) Popovic, D. M.; Stuchebrukhov, A. A. *Biochim. Biophys. Acta, Bioenerg.* **2012**, *1817*, 506-517.

(6) Blomberg, M. R. A.; Siegbahn, P. E. M. *Biochim. Biophys. Acta, Bioenerg.* **2012**, *1817*, 495-505.

(7) Krab, K.; Kempe, H.; Wikstrom, M. *Biochim. Biophys. Acta, Bioenerg.* **2011**, *1807*, 348-358.

(8) Belevich, I.; Bloch, D. A.; Belevich, N.; Wikstrom, M.; Verkhovsky, M. I. *Proc. Natl. Acad. Sci. U.S.A* **2007**, *104*, 2685-2690.

(9) Finklea, H. O. *J. Phys. Chem. B* **2001**, *105*, 8685-8693.

(10) Jeuken, L. J. C.; Jones, A. K.; Chapman, S. K.; Cecchini, G.; Armstrong, F. A. *J Am Chem Soc* **2002**, *124*, 5702-5713.

(11) Leger, C.; Jones, A. K.; Albracht, S. P. J.; Armstrong, F. A. *J Phys Chem B* **2002**, *106*, 13058-13063.

(12) Leger, C.; Bertrand, P. *Chemical Reviews* **2008**, *108*, 2379-2438.

(13) Friedrich, M. G.; Robertson, J. W. F.; Walz, D.; Knoll, W.; Naumann, R. L. C. *Biophys. J.* **2008**, *94*, 3698-3705.

(14) Schach, D.; Nowak, C.; Gennis, R. B.; Ferguson-Miller, S.; Knoll, W.; Walz, D.; Naumann, R. L. C. *J. Electroanal. Chem.* **2010**, *649* 268–276.

(15) Nowak, C.; Laredo, T.; Lipkowski, J.; Gennis, R.; Ferguson-Miller, S.; Knoll, W.; Naumann, R. L. C. *Metallomics* **2011**, *3*, 619–627.

(16) Reinel, D.; Dieterich, W. *J. Chem. Phys.* **1996**, *104*, 5234-5239.

(17) Einax, M.; Solomon, G. C.; Dieterich, W.; Nitzan, A. *J. Chem. Phys.* **2010**, *133*.

(18) Walz, D. *Biochim. Biophys. Acta* **1979**, *505*, 279-354.

(19) Bard, A. J.; Faulkner, L. R. *Electrochemical Methods: Fundamentals and Applications*, 2nd ed.; J. Wiley & Sons: New York, 2001.

(20) Kümmel, R. *Acta Hydrochim. Hydrobiol.* **1988**, *16*, 340.

(21) Naumann, R.; Schiller, S. M.; Giess, F.; Grohe, B.; Hartman, K. B.; Karcher, I.; Koper, I.; Lubben, J.; Vasilev, K.; Knoll, W. *Langmuir* **2003**, *19*, 5435-5443.

(22) Nowak, C.; Santonicola, M. G.; Schach, D.; Zhu, J. P.; Gennis, R. B.; Ferguson-Miller, S.; Baurecht, D.; Walz, D.; Knoll, W.; Naumann, R. L. C. *Soft Matter* **2010**, *6*, 5523-5532.

(23) Hiser, C.; Mills, D. A.; Schall, M.; Ferguson-Miller, S. *Biochemistry* **2001**, *40*, 1606-1615.

(24) Gorbikova, E. A.; Vuorilehto, K.; Wikstrom, M.; Verkhovsky, M. I. *Biochemistry* **2006**, *45*, 5641-5649.

(25) Smirnov, A. Y.; Mourokh, L. G.; Nori, F. *J. Chem. Phys.* **2009**, *130*.

(26) Popovic, D. M.; Stuchebrukhov, A. A. *J. Am. Chem. Soc.* **2004**, *126*, 1858-1871.

(27) Laviron, E.; Meunierprest, R. *J. Electroanal. Chem.* **1992**, *324*, 1-18.

(28) Meunierprest, R.; Laviron, E. *J. Electroanal. Chem.* **1992**, *328*, 33-46.

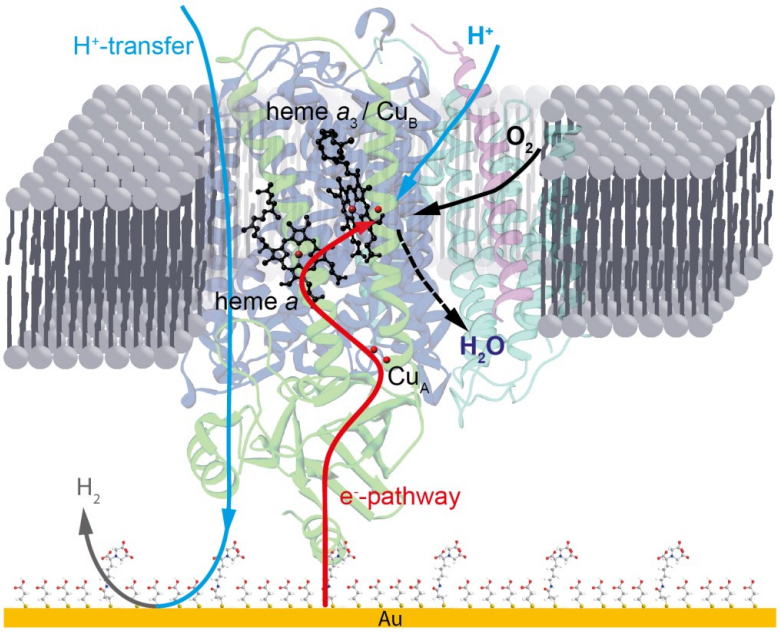

Figure 1: Model system of C*c*O from *R. sphaeroides*, immobilized via his-tag engineered to SU II on an Au electrode and reconstituted into a lipid bilayer.

Figure 2: Reaction scheme of the transition from the oxidized to the reduced state of a single redox couple m considering protonations of oxidized and reduced species. Black arrows show the possible transitions, with the standard redox potentials E_m^0 for the deprotonated species and E_m^{0H} for the protonated species.

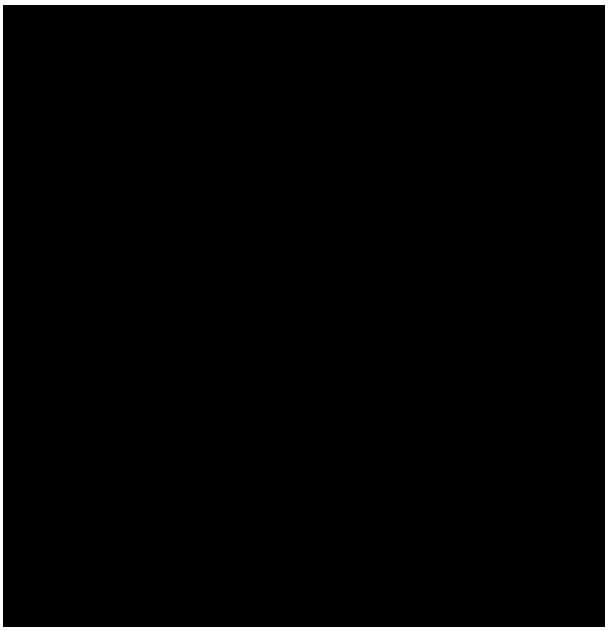

Figure 3: Scheme for second order reaction using total species: Each redox center has four different possibilities to undergo the transition (center l:1-4, center m: 5-8), resulting in 16 different possible combinations.

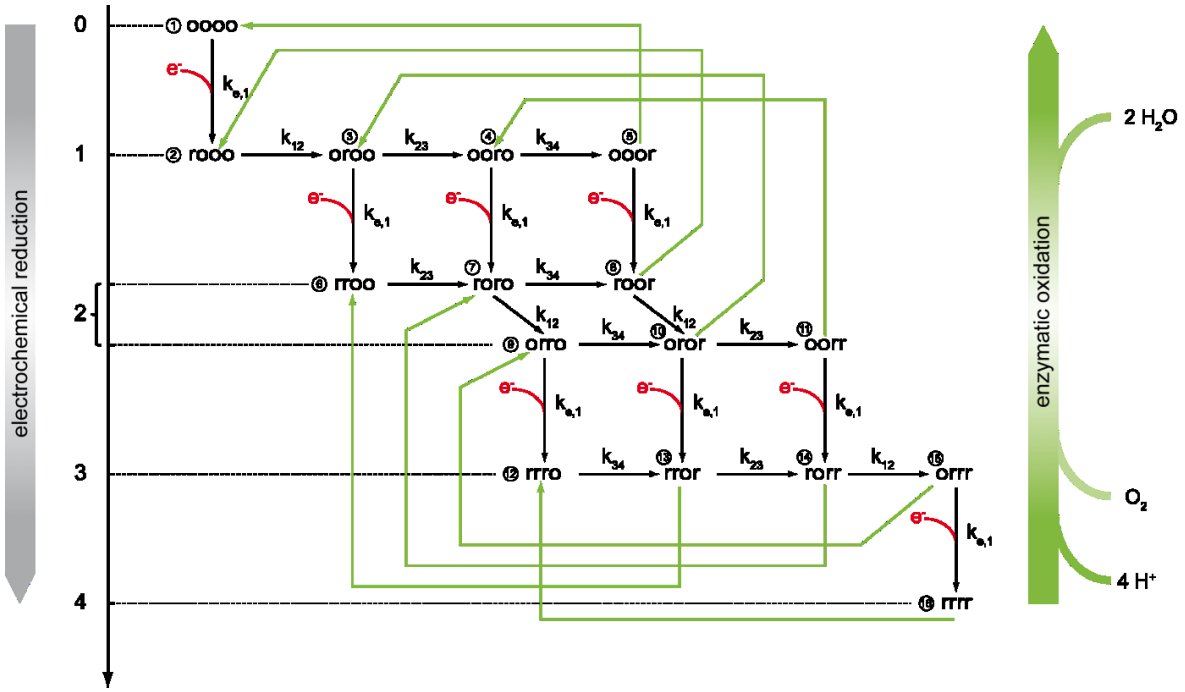

Figure 4: Kinetic scheme for sequential electron transfer in C*c*O under anaerobic and aerobic conditions. The four centers are arranged in the order Cu_A, heme *a*, heme a_3 and Cu_B, which can be present either in the reduced (r) or oxidized (o) state. All of the r and o states can be protonated or deprotonated. Hence, the enzyme can exist in 16 different redox states and 256 protonation states. Vertical arrows with red branches represent electron uptake from the electrode, while black horizontal arrows indicate second order reactions between redox centers. Green arrows show enzymatic reoxidation under aerobic conditions. Oxidation steps start with Cu_B in the reduced state. Different oxidized states of the enzyme are thus restored.

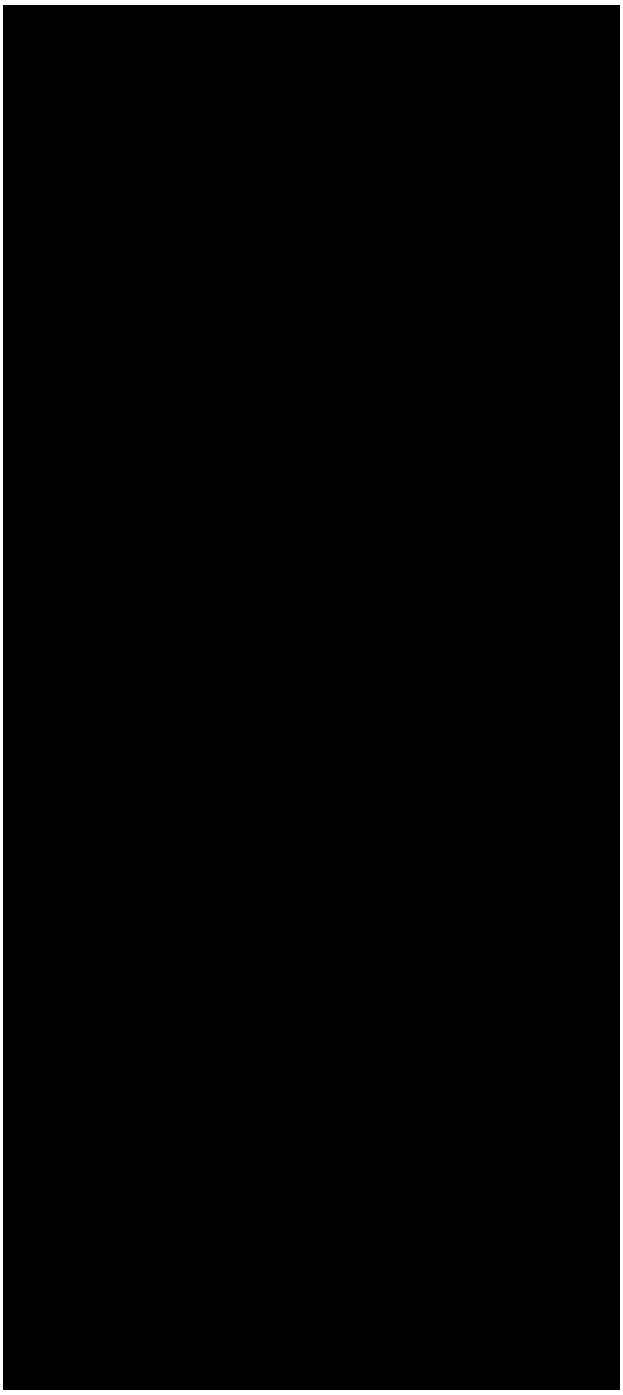

Figure 5: Experimentally measured CVs of C*c*O under anaerobic (A,C) and aerobic (B) conditions in the non-activated (A) and activated (B,C) state, respectively. The insets show baseline corrected signals, normalized to the same scan rate ($50\ \mathrm{mV} \cdot \mathrm{s}^{-1}$) in order to exclude charging effects of the ptBLM and the electrochemical reduction of oxygen at the electrode.

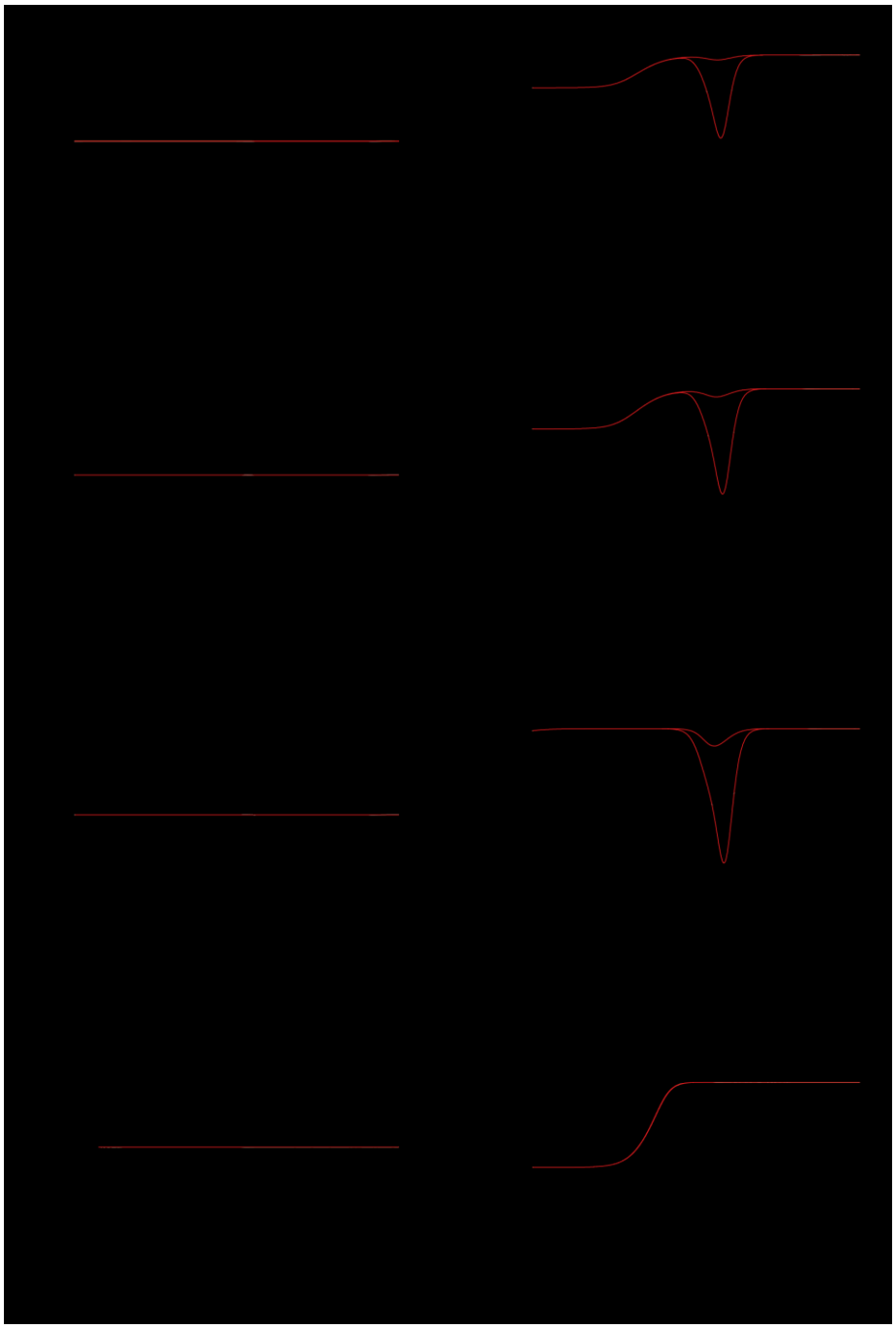

Figure 6: CVs simulated under anaerobic conditions (A,C,E,G) and under aerobic conditions (B,D,F,H). Different parameter sets for the acid dissociation constants are used, see Table 1 (V1=A,B,G,H / V2=C,D / V3=E,F). The black lines represent the overall currents, while the red lines show currents resulting from proton reaction with the electrode. (G) and (H) show simulation results using the activated standard redox potentials for anaerobic and aerobic conditions respectively.